Carbon 234 (2025) 119952

Contents lists available at ScienceDirect

Carbon

journal homepage: www.elsevier.com/locate/carbon

Cumulenic *sp*-Carbon atomic wires wrapped with polymer for supercapacitor application

Subrata Ghosh [a,*], Massimiliano Righi [a], Simone Melesi [a], Yu Qiu [b], Rik R. Tykwinski [b], Carlo S. Casari [a,**]

[a] Micro and Nanostructured Materials Laboratory — NanoLab, Department of Energy, Politecnico di Milano, Via Ponzio 34/3, Milano, 20133, Italy
[b] Department of Chemistry, University of Alberta, Edmonton, Alberta, T6G 2G2, Canada

ARTICLE INFO

Keywords:
Carbyne
Nanocarbons
Micro-supercapacitor
Energy storage

ABSTRACT

Carbyne, the ideal linear atomic wire consisting of a single-atom thick chain of *sp*-carbon, is theoretically predicted to have around five times higher surface area than graphene, notable charge mobilities, as well as excellent optical and thermal properties. Despite these impressive properties, the exploitation of carbyne-like system as an electrochemical energy-storage electrode has not been reported so far. To address this challenge, we focused on experimentally available finite and short linear atomic chain of *sp*-carbon. Herein, we prepare solution-processed thin films of tetraphenyl [3]cumulenic *sp*-carbon atomic wires embedded in a polymer matrix, in which *sp*-carbon atomic wires feature three cumulated carbon-carbon double bonds terminated at each end by two phenyl groups. Raman and UV–visible spectroscopy confirms the presence of *sp*-carbons inside the polymeric matrix. Finally, we investigate the supercapacitor performance of cumulenic *sp*-carbon atomic wires embedded polymer in three aqueous electrolytes, namely 1 M Na_2SO_4 (neutral), 1 M H_2SO_4 (acidic), and 6 M KOH (basic). The results suggest 6 M KOH is the best electrolyte to obtain high charge-storage performance of device with areal capacitance of 2.4 mF/cm^2 at 20 mV/s, 85 % cycle stability after 10000 charge-discharge cycles, and excellent frequency response.

1. Introduction

The electrochemical capacitor or supercapacitor is anticipated as a promising electrochemical energy device to store the charge from renewable energy sources as well as high-power applications that require rapid on–off response such as hybrid electric vehicles, forklifts, load cranes, grid stabilization systems, etc. [1] Since the charge-storage mechanism is completely physical, unlike the chemical storage mechanism in batteries, a supercapacitor is well-known for the excellent power density, cycle stability, safety, and capability to work in a broad temperature range (−10 to 100 °C). However, low energy density restricts its use only for high-power applications. To improve the energy density of supercapacitors, one can increase the capacitance by tuning the porosity and structural properties of electrode materials, by doping or decorating carbon-nanostructures, or using electrolytes to increase the voltage of the device, and choosing the best electrode-electrolyte combination to obtain better charge-storage performances [2–4].

There is extensive research on materials for supercapacitor electrodes starting from nanocarbons, 2D materials (e.g., MXene, transition metal dichalcogenides), conducting polymers, and their composites [2–7]. Amongst these, carbon-based materials come to the spotlight due to their high surface area, controllable porosity, excellent structural properties like electrical conductivity and thermal conductivity, and excellent stability. On the other hand, low density of states, chemical inertness, low packing density, and poor wettability are the limiting factors to obtain high charge storage performances. Among the carbon-based materials, graphene, which is 100 % sp^2-hybridized carbon, has a high surface area (2630 m^2/g) and excellent properties, but the predicted specific capacitance of 550 F/g has not achieved so far. The KOH activation of microwave exfoliated graphene oxide (98 % sp^2-carbon) has been reported as an excellent supercapacitor electrode. A microwave exfoliated graphene oxide electrode with specific surface area of 3100 m^2/g delivered the gravimetric capacitance of 200 F/g at the current density of 0.7 A/g [8] However, the small overpotential of

* Corresponding author.
** Corresponding author.
E-mail addresses: subrata.ghosh@polimi.it, subrata.ghoshk@rediffmail.com (S. Ghosh), carlo.casari@polimi.it (C.S. Casari).

https://doi.org/10.1016/j.carbon.2024.119952
Received 1 December 2024; Received in revised form 17 December 2024; Accepted 19 December 2024
Available online 20 December 2024
0008-6223/© 2024 The Authors. Published by Elsevier Ltd. This is an open access article under the CC BY license (http://creativecommons.org/licenses/by/4.0/).

oxygen and hydrogen evolution reaction of sp^2-carbons in aqueous electrolyte often restricts the operating voltage window within 1.23 V during the charge-discharge process. On the other hand, diamond (sp^3-hybridized carbon) is promising and can operate in a widen potential window both in aqueous and non-aqueous electrolytes with excellent electrochemical stability [9,10]. However, the specific capacitance of diamond-based structures is quite low. Thus, the attention has turned to sp^2-sp^3 hybrid carbon structures of as materials energy storage electrode. It has been reported, for example, that Q-carbon microdots (81.3 % sp^3-hybridized carbon) delivers higher charge-storage performance than other carbon structures, including Q-carbon filament (78.3 % sp^3-carbon) and Q-carbon cluster (73 % sp^3-carbon) [11].

Apart from sp^2-and sp^3-hybridized carbon, *sp*-carbon offers other appealing opportunities in the form of carbon atomic wires (CAWs) modeling the elusive carbon allotrope carbyne. It has been predicted that the carbyne, the ideal infinite linear chain of *sp*-carbon atoms, has a high theoretical surface area of more than 13000 m^2/g for H_2 storage, which is much greater than graphene (2630 m^2/g) [12]. Carbyne should also possess excellent thermal conductivity (80 ± 26 kW/m/K at room temperature) [13] and electronic mobility (>10^5 cm^2/Vs) [14,15]. Based on the bonding arrangement in the linear *sp*-carbon chain, carbyne has two possible structures: (a) polyynes with alternating single and triple carbon-carbon bonds and a semiconducting behavior and (b) cumulenes with contiguous double bonds and metallic behavior [16]. Experimentally, as finite strands of carbyne short chain are synthesizable up to several tens of atoms for polyynes and just a few atoms for cumulenes due to their high reactivity [17]. Longer chains approaching the ideal carbyne are achieved only when encapsulated in carbon nanotubes thus forming a hybrid *sp*-sp^2 system. Isolated *sp*-carbon chains have been obtained only in the form of carbon atomic wires (CAWs) with finite lengths and with different endgroups (e.g., H, CN, methyl, aryl, halogen) [18–20]. The choice of the chain length and the end-group are fundamental since both can affect the stability and the tunability of the optoelectronic properties of these *sp*-carbon systems. The optical energy gap can be modulated by varying the number of *sp*-carbons in the chain (i.e., longer chains present a lower optical gap) and by changing the endgroups [18,21,22]. Bulkier endgroups increase the stability of these systems [17]. Another possibility to protect CAWs is their embedding inside polymeric matrices [23–25] avoiding exposure to detrimental environmental agents, reducing their mobility, and diminishing the tendency of crosslinking among adjacent *sp*-carbon chains that leads to more stable sp^2 structures [26–28].

CAWs and other carbon-based materials with an increasing proportion of *sp*-hybridized are attractive to researchers for hydrogen storage [12], electrochemical energy storage [29], field effect transistors [30], and organic electronic applications [31]. It has been reported that the *sp*-carbon content in nanothick amorphous carbon coating has strong influence on its mechanical properties [32]. *sp*-carbon rich films have been explored as a supercapacitor electrode in ionic electrolyte with maximum areal capacitance of 0.32 mF/cm^2 at 0.05 V/s with respect to the reference electrode [29]. In another study, carbon coated Ni foam is reported to deliver an areal capacitance of 53.06 mF/cm^2 at 5 mV/s in 1 M Na_2SO_4 with respect to the reference electrode [33]. This latter study [33], however, presents some concerns regarding the reporting of the specific capacitance below 20 mV/s which may not be appropriate, and the shape of the CV traces is not ideal for supercapacitor. Moreover, Raman peaks at 1143.5 cm^{-1} and 1539.8 cm^{-1} are attributed to the β-carbyne (cumulenic carbyne), and carbon networks (*sp*-, sp^2-, and sp^3-carbon), respectively, while the main peaks in Raman spectra for *sp*-carbon should be in the range of 1800 and 2300 cm^{-1} [34]. In our previous study [35], we investigated carbon nanofoam containing *sp*-, sp^2-, and sp^3-carbon with hydrogen, nitrogen, and oxygen functionalization for supercapacitor applications. However, the content of *sp*-carbon is very low and its exact role on the supercapacitor performance is not clear.

In this work, we chose a cumulenic CAW system with three cumulated carbon-carbon double bonds terminated at each end by two phenyl groups ([3]Ph-cumulene). We produced a polymeric thin film embedding -[3]Ph-cumulene into poly (methyl methacrylate) (PMMA), and we investigated the charge-storage performance and frequency response of cumulenic *sp*-carbon atomic wires-based symmetric supercapacitor devices in three different aqueous electrolytes (1 M Na_2SO_4, 1 M H_2SO_4 and 6 M KOH). We also investigated the structural stability of [3]Ph-cumulene after electrochemical measurements by Raman spectroscopy.

2. Experimental details

The [3]Ph-cumulene electrode is synthesized using a blend of PMMA/[3]Ph-cumulene in N,N-Dimethylformamide (DMF, HPLC grade ≥99.7 %, Alfa Aesar). The composition of these films was optimized to achieve the highest possible concentration of [3]Ph-cumulene relative to PMMA while maintaining a minimum amount of polymer. The mixture was prepared by dissolving 0.02 g of PMMA powder in 1 mL of DMF, achieving complete dissolution through stirring at 50 °C for 3 h. Separately, a second solution containing the cumulene was prepared by dissolving 8 mg of [3]Ph-cumulene powder in 1 mL of DMF, ensuring homogeneity through stirring and heating at 40 °C for 3 h. To maximize the concentration of [3]Ph-cumulene, this solution was brought close to its solubility limit in DMF. The two homogeneous solutions were then mixed and stirred for 3 h at 30 °C. A drop of the resulting solution was drop-cast onto a carbon-paper substrate, and gentle evaporation of the solvent was achieved by placing the sample under a vented chemical hood. After complete solvent evaporation, the drop-casting process was repeated until a film of sufficient thickness (>1 mg/cm^2) was obtained.

Raman spectra of the pure powder of [3]Ph-cumulene and of [3]Ph-cumulene embedded within the PMMA film – both before and after electrochemistry measurements - have been acquired with a Renishaw inVia Raman microscope with a diode-pumped solid-state laser with two possible wavelengths (λ = 532 or 660 nm). All the spectra were acquired with a 532 nm excitation laser and with 500 accumulations of 0.1 s each. The laser power was set to 0.7 mW to avoid degradation of the cumulene during the measurements. To address the inhomogeneities in the [3]Ph-cumulene wrapped PMMA, spectra were averaged by measuring at various spots across the film.

UV–Vis absorption spectra of [3]Ph-cumulene were recorded dissolving the cumulene powder in DMF. The final concentration was about 10^{-5} M. Spectra were recorded at room temperature using a Shimadzu UV-1800 UV/Visible scanning spectrophotometer with a detection range of 190–1100 nm. The sampling interval of the spectra was set to 0.2 nm. The sample solution was analyzed inside a quartz cuvette with a 10 mm optical path.

The electrochemical charge-storage performances of the samples were conducted in Swagelok Cell (SKU: ANR-B01, Singapore) and three standard aqueous electrolytes, namely 1 M Na_2SO_4, 1 M H_2SO_4, and 6 M KOH, are used. The hydrophobic polypropylene (PP) membrane was modified by a two-step process: soaked with acetone at 20 °C for 5 min and followed by aqueous 6 M KOH solution at 20 °C, and used after 1 h [51]. The cell was assembled by sandwiching separator-soaked-electrolytes between as-prepared electrode material grown on carbon paper. For the electrochemical testing, electrode materials and modified separator were dipped into the electrolyte solution for 1 h. Cyclic voltammogram, charge-discharge test, and electrochemical impedance spectra were recorded using a PALMSENS electrochemical workstation. The cyclic voltammetry at different scan rates ranging from 20 to 1000 mV/s and charge-discharge at different current densities of 150–500 μA were carried out and scanned within the defined voltage at 100 mV/s for 1000 times. The areal capacitance is calculated using the equation: $C_{areal} = \int I\,dV / A.\,v.\Delta V$, where I is the current, v is the scan rate, A is the geometric area of the electrode and ΔV is the voltage of the device. Single electrode capacitance = 4 × device

capacitance. The volumetric capacitance of electrode materials is estimated by dividing the areal capacitance by the total height of two carbon nanofoam electrodes. The electrochemical impedance spectroscopy is conducted in the frequency range of 1 Hz to 0.1 MHz at open circuit potential with a 10 mV *a. c.* Perturbation. The energy density (E_A) of the device is calculated via the equation: $E_A = C_{dl}V^2/2$, where C_{dl} is the double layer capacitance at 120 Hz obtained from the areal capacitance versus frequency plot. The relaxation time constant is calculated from the impedance spectra at 120 Hz using the equation: $\tau_{RC} = -Z'/2\pi f Z''$, where Z′ and Z″ are the real and imaginary components of impedance, respectively.

3. Results & discussions

The electrode material based on [3]Ph-cumulene wrapped poly (methyl methacrylate) (PMMA) is prepared by embedding the [3]Ph-cumulene within PMMA a drop cast thin film on a carbon paper substrate (Scheme 1, see Experimental section for further details). The symmetric device is assembled by two identical electrodes and separator-soaked-electrolyte.

To ensure the correct embedding and to verify that the [3]Ph-cumulene retained its properties during processing, Raman spectroscopy has been performed on the pure PMMA powder [3]Ph-cumulene powder, and on the [3]Ph-cumulene wrapped PMMA film. The Raman spectrum are shown in Fig. 1a. The spectrum of PMMA is characterized mainly by three peaks in the region of 2800–3000 cm^{-1} that are associated with the CH stretching of the polymeric chain. The Raman spectra of [3]Ph-cumulene consist of a strong peak at 2035 cm^{-1} related to the Effective Conjugation Coordinate (ECC) normal mode, a collective vibration of all the *sp*-carbon atoms in the chain [22]. At 1593 cm^{-1}, the [3]Ph-cumulene presents another remarkable peak associated with the stretching mode of the phenyl endgroups. In the spectrum of the [3]Ph-cumulene wrapped PMMA film, the cumulenic Raman modes remain prominent and suggest that the cumulene is stable and degradation does not occur during the preparation of the samples. Interestingly, in this spectrum, the PMMA peaks are barely distinguishable. This can be explained both considering the high concentration of cumulene powder in the films and the very high Raman scattering cross-section of cumulenes over the polymer [36]. From the UV–vis absorption spectra, we verified the structure of [3]Ph-cumulene with three absorption bands observed at 415, 317, and 270 nm (Fig. 1b) [30,37]. Notably, the UV–vis spectra of [3]Ph-cumulene and [3]Ph-cumulene + PMMA show nearly identical profiles suggesting that PMMA does not affect the optical properties of [3]Ph-cumulene.

The charge-storage performance of [3]Ph-cumulene wrapped PMMA supercapacitor devices is investigated in three different aqueous electrolytes, namely H_2SO_4 (acidic), Na_2SO_4 (neutral), and KOH (basic). Fig. 2a shows the representative cyclic voltammograms (CVs) of symmetric device with 1 m Na_2SO_4 electrolyte at different scan rates in the range of 0.2 mV/s to 1 V/s. The CV analyses of the devices in 1 m H_2SO_4 and 6 m KOH are shown in Figs. S1a–b. The CV profile is found to be near-rectangular and mirror symmetric for all scan rates indicating excellent supercapacitor behavior. The noticeable difference in the CV for different electrolytes is their capability to work at different voltages (Fig. 2b). We compared this device performance when adopting a pure PMMA electrode without [3]Ph-cumulene. The plot of areal capacitance versus scan rate for the PMMA/6 m KOH/PMMA symmetric device is provided in Fig. S1c, and the areal capacitance is determined to be much lower than the [3]Ph-cumulene wrapped PMMA symmetric device at the given scan rate. The [3]Ph-cumulene wrapped PMMA in Na_2SO_4 can sustain the voltage of 1 V, the stable voltages of devices for 1 m H_2SO_4 and 6 m KOH is found to be 0.8 V without observable evolution of oxygen and hydrogen. At 0.1 V/s, the energy density of all devices is found to be around 0.11 μWh/cm^2. This result suggests that the use of Na_2SO_4 electrolyte may not be a great option despite a widened stable voltage is achieved. Thus, it is important to inspect other parameters like rate performance, cycle stability, and charge-storage kinetics of the electrode under different electrolytes. The areal capacitance of the devices in different aqueous electrolytes is estimated and plotted with respect to the scan rate (Fig. 2c). The highest areal capacitance of device is obtained in 6 m KOH (2.4 mF/cm^2) and in H_2SO_4 (2.8 mF/cm^2), whereas the lowest is observed in Na_2SO_4 (2 mF/cm^2), with all measurements at the scan rate of 0.02 V/s. This higher specific capacitance of the [[3]Ph-cumulene wrapped PMMA in KOH and H_2SO_4 electrolyte over Na_2SO_4 can be attributed to the lower ionic radius and higher ionic mobility of H^+-ions for [3]Ph-cumulene wrapped PMMA film/H_2SO_4, and better wettability of KOH and higher K^+-ion diffusion for [3]Ph-cumulene wrapped PMMA in KOH [38]. At 0.1 V/s scan rate [3]Ph-cumulene wrapped PMMA (areal capacitance of electrode = 4 × specific capacitance of device = 5.2 mF/cm^2) outperforms values reported for vertical

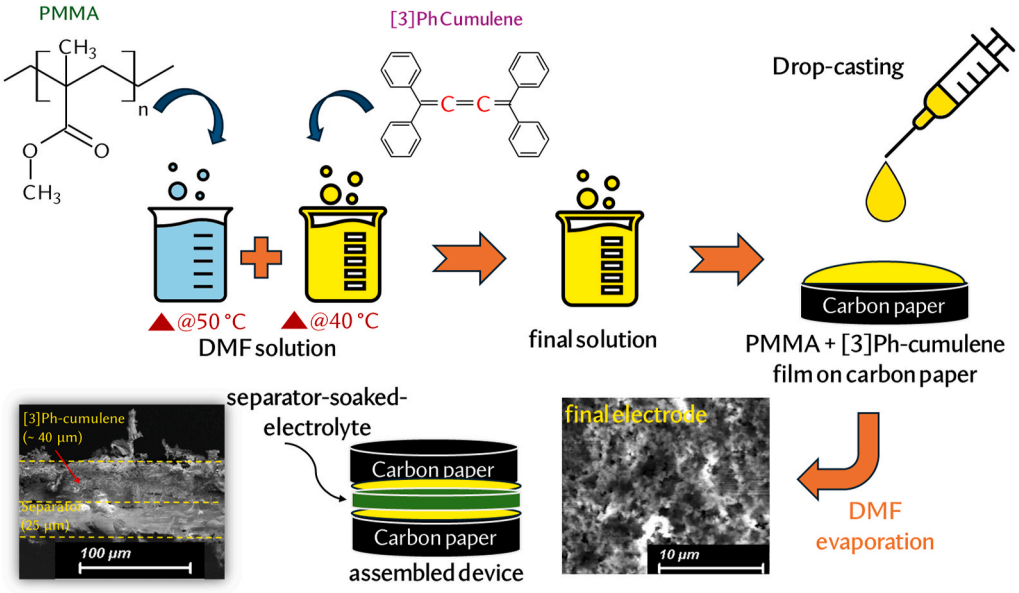

Scheme 1. Schematic of [3]Ph-cumulene-PMMA electrode fabrication. The top view of final electrode and the cross-sectional scanning electron micrographs of thin film electrode on separator are provided at the bottom panel.

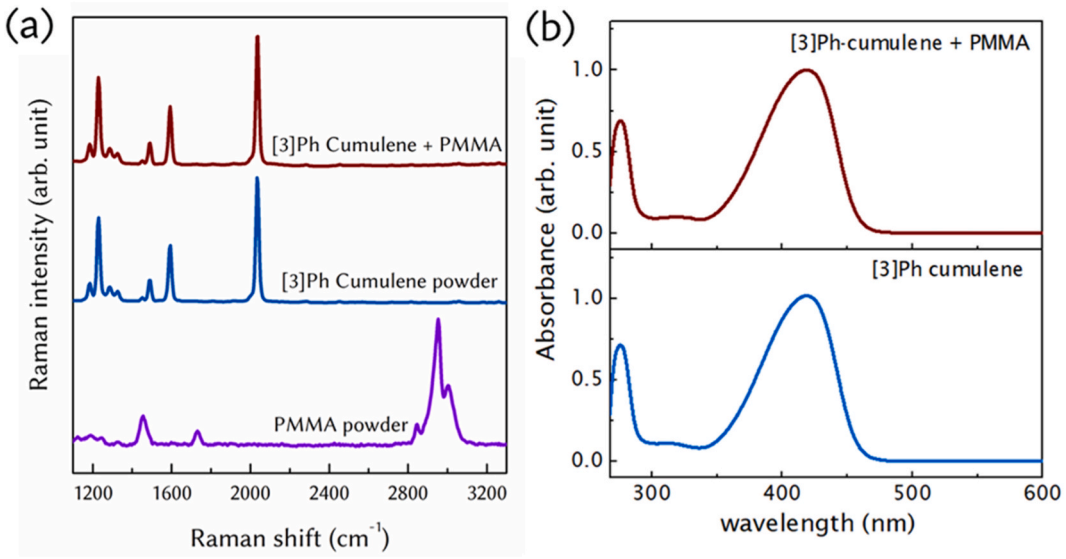

Fig. 1. (a) Raman spectra of PMMA powder (purple) -[3]Ph-cumulene powder (blue), and drop casted thin film of [3]Ph-cumulene wrapped with PMMA (red). (b) UV–Vis absorbance spectra of the [3]Ph-cumulene (in DMF) and [3]Ph cumulene wrapped PMMA (in DMF); DMF: N,N-dimethylformamide. (For interpretation of the references to colour in this figure legend, the reader is referred to the Web version of this article.)

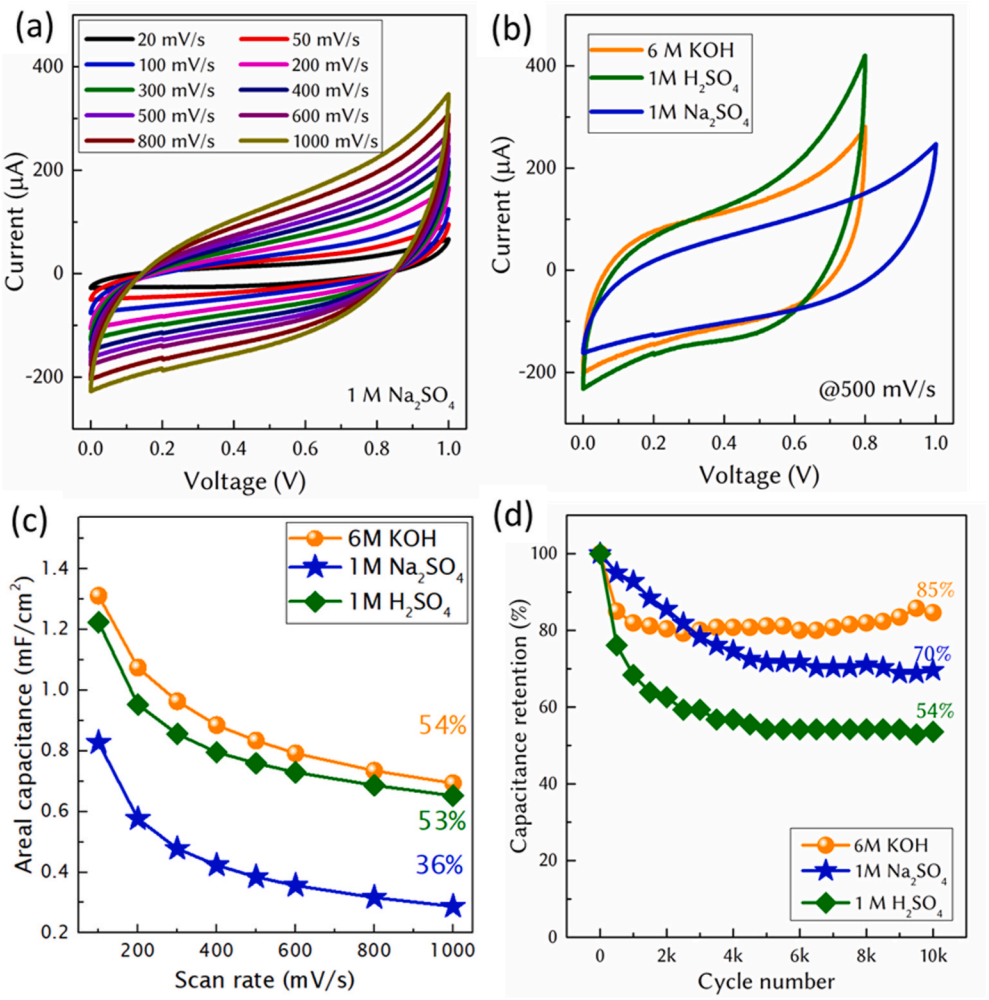

Fig. 2. Charge-storage performance of carbyne. (a) Cyclic voltammogram of a symmetric device [3]Ph-cumulene in 1 m Na_2SO_4, (b) comparative voltammogram of the devices in 1 M Na_2SO_4, 1 M H_2SO_4, and 6 M KOH. Aqueous electrolyte dependent (c) areal capacitance with respect to the scan rate and their (d) cycle stability. (A colour version of this figure can be viewed online.)

graphene nanosheets (0.197 mF/cm^2) [38], carbon/metal oxynitride nanofoam composite (2.4 to 7.4 mF/cm^2) [39], $Ni_3(HHTP)_2$@woven fabrics (0.205 mF/cm^2), TiO_2 nanogrids (0.74 mF/cm^2) [40], and titanate hydrate nanogrids (0.08 mF/cm^2) (Table 1) [40]. At 1 V/s scan rate, the areal capacitance of [3]Ph-cumulene wrapped PMMA is found to be 2.8 mF/cm^2 in 6 M KOH, which is higher than the previously reported *sp*-carbon-rich nanostructured materials (264 μF/cm^2) and carbyne-depleted nanostructured carbon (234 μF/cm^2) at 1 V/s for in 1-ethyl-3-methylimidazolium bis(trifluoromethylsulfonyl)imide ionic electrolyte in three-electrode system (both values are derived here from data extracted from the plots in Ref. [29]).

The rate performance shows that the [3]Ph-cumulene wrapped PMMA device in 6 M KOH, 1 M H_2SO_4 and 1 M Na_2SO_4 maintain 54 %, 53 %, and 36 % at 1 V/s, respectively, compared to the areal capacitance measured at 0.1 V/s (36 %). The charge-discharge profiles of the devices at different current densities are shown in Figs. S1d–f, and the profiles are found to be symmetric and near-linear for all the cases, which is in good agreement with the CV results. Interestingly, the [3]Ph-cumulene wrapped PMMA in 6 M KOH stands out as more stable when compared to the other two after 10 000 charge-discharge cycles. A closer inspection indicates an increased cycle stability of [3]Ph-cumulene wrapped PMMA in 6 M KOH over prolonged charge-discharge cycles after an initial decrease, which can be attributed to the electrochemical activation of electrode materials during the charge-discharge process [35].

The better rate performance and cycle stability of the [3]Ph-cumulene wrapped PMMA film in 6 M KOH compared to that in 1 M H_2SO_4 could be due to the balance between the contribution arising from double layer capacitance and pseudo-capacitance. Conducting polymer-based materials (as PMMA in our case) are well known to contribute pseudo-capacitance, and carbon-based materials (e.g., cumulenic *sp*-carbon here) provide double-layer capacitance. It should also be noted that the functional groups attached to the carbon surface (phenyl groups for cumulene in our case) also contribute to the pseudocapacitance [2]. In order to estimate both contributions, using the partition procedure by Trasatti method analysis [41,42], double-layer capacitance is estimated from a plot of C_A vs $\nu^{-1/2}$ (Fig. 3a), and the total capacitance is estimated from the plot of $1/C_A$ vs $\nu^{1/2}$ (Fig. 3b). The pseudo-capacitance is estimated from the difference between total capacitance and double-layer capacitance. Interestingly, it has been seen that the [3]Ph-cumulene wrapped PMMA provides higher double-layer capacitance contribution in 6 M KOH (Fig. 3c) than that in 1 M H_2SO_4, and, hence, better stability is obtained.

Spectroscopic investigation of electrochemical impedance is carried out to probe further on the charge-storage kinetics, frequency response, and possibility of utilization for applications in AC line filtering. The characteristics needed for filtering are a small resistor-capacitor time constant (τ_{RC}), small characteristic relaxation time constant at −45° (τ_0), large areal capacitance, and small phase angle obtained at 120 Hz (2nd harmonic of 60 Hz AC frequency, US standard). The characteristic relaxation time constant at −45° (τ_0) represents the time needed when the discharge of the device goes 50 % of maximum efficiency, where −45° is the boundary between capacitive and resistive behavior [43]. The resistor-capacitor time constant (τ_{RC}) is the time needed to charge 63.2 % of the full potential of the capacitor.

From the Nyquist plot (Fig. 4a), the lowest equivalent series resistance (ESR) of [3]Ph-cumulene wrapped PMMA film is achieved in 6 M KOH (0.8 Ω) compared to that in 1 M Na_2SO_4 (4.6 Ω), and 1 M H_2SO_4 (1.7 Ω). Moreover, no semicircle is observed in the high-frequency zone of Nyquist plot indicating negligible charge-transfer resistance and hence excellent Ohmic contact between the electrode materials and current

Table 1
Comparison of thin film microsupercapacitor devices with frequency response (* represents the calculated value using the data available in the cited reference) To quantify the areal capacitance of electrode material, one need to multiply the areal capacitance of device by 4. (in table, 3 E: three electrodes, $EMIMBF_4$: ethyl-3-methylimidazolium tetrafluoroborate, $EMImNTf_2$: 1-ethyl-3-methylimidazolium bis(trifluoromethane sulfonyl)imide; $TEABF_4$: Tetraethylammonium tetrafluoroborate, AN: acetonitrile).

Electrode materials	Electrolyte	Areal capacitance of device (electrode) in mF/cm^2	Areal capacitance at 120 Hz (EIS) (μF/cm^2)	Negative phase angle at 120 Hz (°)	Frequency (Hz)/ Relaxation time constant (ms) at −45°	resistor-capacitor time constant at 120 Hz (ms)	Cyclic stability
Cumulenic *sp*-Carbon Atomic Wires - This work	1 M Na_2SO_4	0.8 (3.2) at 0.1 V/s	22	50	1000/1	1.04	54 % after 10^5 cycles at 100 μA
	1 M H_2SO_4	1.2 (4.8) at 0.1 V/s	66	51	756/1.3	1.04	70 % after 10^5 cycles at 100 μA
	6 M KOH	1.3 (5.2) at 0.1 V/s	177	52.8	1301/0.7	1.14	85 % after 10^5 cycles at 100 μA
Carbon foam thickness ~8.6 μm [35]	6 M KOH	0.9 at 0.1 V/s	134	54.04	1321.9/0.86		104 % after 10^5 cycles at 125 μA
carbonized melamine foams [56]	1 M $TEMABF_4$/AN	–	132	80.1	-/0.352		87.4 % after 10^5 cycles at 10 mA/cm^2
3D ordered porous graphene [49]	0.1 M $LiClO_4$	3.8 at 25 μA/cm^{-2} (current density is too low)	755	53	-/1.46	0.98	96.7 % after 500 μA/cm^{-2}
Graphite@N-doped diamond nanoneedles [57]	1 M Na_2SO_4 in 3 E	0.126 (0.1 V/s)	–	–	–		100 % (10 000 cycles, 0.02 mA cm^{-2})
	0.1 M $TBABF_4$ in PC, 3 E	0.06 (0.1 V/s)	–	–	–		
Vertically oriented graphene [58]	25 % KOH	–	87	82	15 000/0.067		–
Carbon nanotube [59]	$EMImNTf_2$	–	128	80.1	-/0.794		–
pristine carbon [60]	1 M $TEABF_4$ in	–	444	80	890/1.2	–	–
N-doped carbon [60]	AN	–	545	67	280/0.56	–	–
P/N-doped carbon [60]		–	30	82	13 200/0.077	–	–
B/N-doped carbon [60]		–	99	83	5200/0.2	0.13	–
laser-processed carbon-titanium carbide [61]	$EMIMBF_4$	–	118	61.5	1121.3/0.89	0.7	100.95 % after 14 000 cycles at 10 V/s

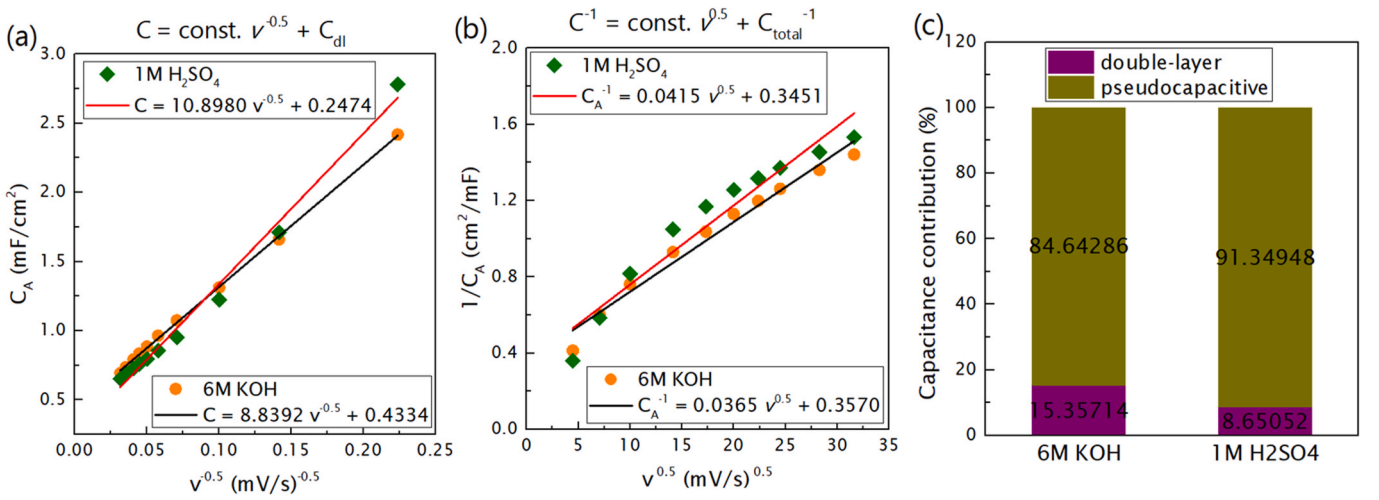

Fig. 3. Plot of (a) areal capacitance (C_A) versus reciprocal square roots of scan rate ($\nu^{-1/2}$), and (b) reciprocal of areal capacitance vs $\nu^{1/2}$. (c) Estimated double-layer capacitance and pseudocapacitance contribution of the [3]Ph-cumulene wrapped PMMA in 6 M KOH and 1 M H_2SO_4. Solid lines in (a–b) represent linear fitting and the corresponding fitting equation is provided as an inset. C_{dl} and C_{total}, presented in the equation (on the top of figure a–b) are the double-layer and total capacitance of the device, respectively. (A colour version of this figure can be viewed online.)

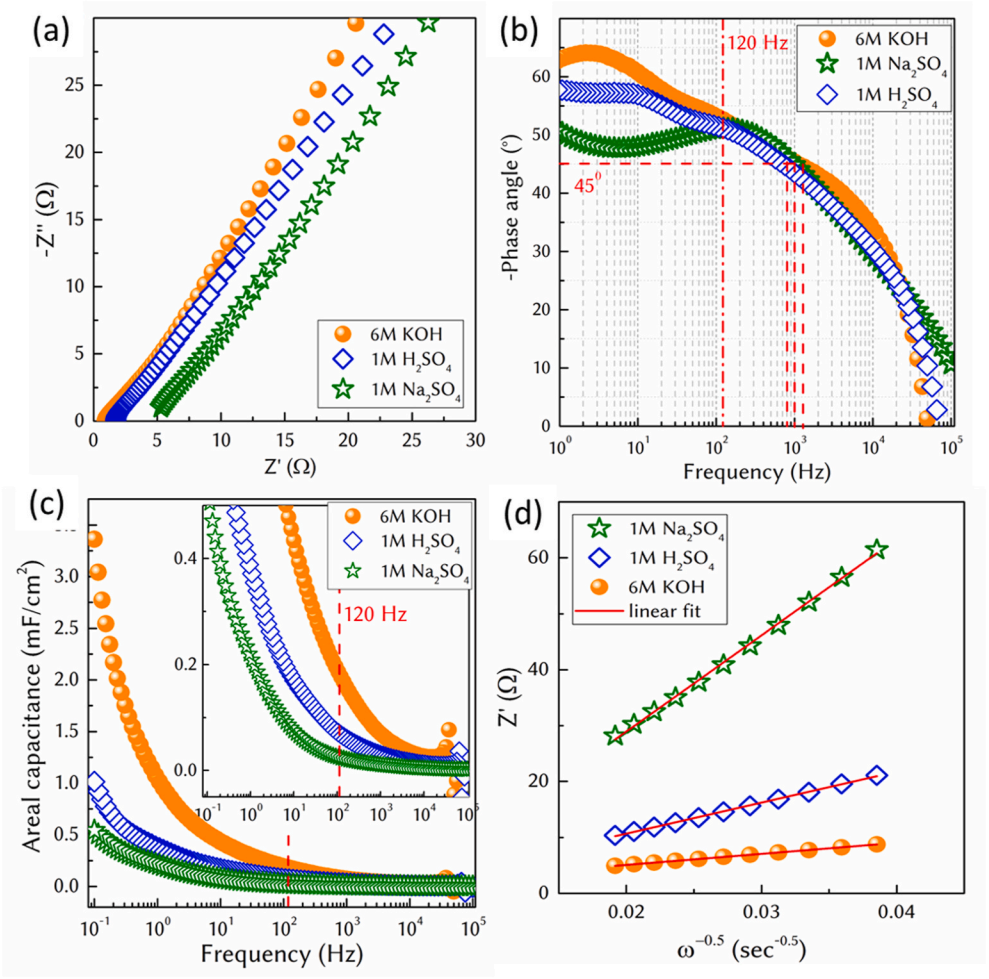

Fig. 4. Frequency response. (a) Nyquist plot, (b) Bode plot, (c) frequency dependent areal capacitance, and (d) plot of Z′ vs $\omega^{-0.5}$ of [3]Ph-cumulene wrapped PMMA supercapacitor in 1 M Na_2SO_4, 1 M H_2SO_4, and 6 M KOH. (A colour version of this figure can be viewed online.)

collector, fast electrochemical reaction rate and/or fast charge-transfer kinetics for all devices [38]. The Bode plot for each device is shown in Fig. 4b. At 120 Hz, the negative phase angle for the [3]Ph-cumulene wrapped PMMA film in 6 M KOH, 1 M H_2SO_4, and 1 M Na_2SO_4 is 52.8°, 51°, and 50°, respectively. Although the negative phase angles of our device at 120 Hz is lower than the ideal capacitor (90°) or vertically oriented graphene (85°) [44], it is comparable and/or better than *N*-doped mesoporous carbon (0°) [45], activated carbon-based commercial electric double layer capacitor (0°) [46,47], thermally reduced graphene oxide (30°) [48], 3D ordered porous graphene film (53°) [49], and carbon nanowall foam (47°) [50]. Moreover, it has been demonstrated for $NiTe_2$-based devices that the negative phase angle around 53° is sufficient for the AC line filtering applications [51]. The areal capacitance at 120 Hz of [3]Ph-cumulene wrapped PMMA supercapacitor device (C_{dl}) obtained in 1 M Na_2SO_4, 1 M H_2SO_4, and 6 M KOH are 22, 66, and 177 μF/cm^2, respectively (Fig. 4c). It has been reported that by reducing the thickness of a carbon nanotube film from 300 nm (loading ~32 μg/cm^2) to 50 nm (~4 μg/cm^2), the negative phase angle increases from 70.6° to 82.7°, and the areal capacitance decreases from 233 to 43 μF/cm^2. These results also indicate that using a thinner separator provides higher areal capacitance and negative phase angles [52]. In our case, the mass loading of material is much higher (1 mg/cm^2) than in Ref. [52]. Decreasing the electrode thickness may be the plausible solution to increase the negative phase angle at 120 Hz [53], which is in the scope of our future research. The maximum areal capacitance obtained for [3]Ph-cumulene wrapped PMMA film in 1 M Na_2SO_4, 1 M H_2SO_4, and 6 M KOH are 0.42, 0.79 and 2.63 mF/cm^2, respectively at the lowest frequency (Fig. 4c).

The characteristics time constants (τ_0) and capacitor-resistor time constant (τ_{RC}) are estimated for all devices from the impedance spectroscopic data. The estimated τ_0 for KOH, H_2SO_4, and Na_2SO_4 are 0.7, 1.3 and 1 ms, respectively and the corresponding characteristics frequency (f_0) at −45° are 1301 Hz, 756 Hz, and 1000 Hz. The capacitor-resistor time constant of our devices is 1.14, 1.04, and 1.04 ms in KOH, H_2SO_4, and Na_2SO_4, respectively, which is ~3 orders of magnitude smaller than that of the commercial ECs (~1 s) [54]. The small values of τ_{RC} and τ_0 for our devices suggest ultrafast frequency response.

The real part of impedance (Z′) is related to ion migration, electrical conduction, and ion diffusion. The slope of the curve represents the diffusion impedance. Since the active material is the same [3]Ph-cumulene wrapped PMMA film, electrical conductivity is assumed to be the same for all identical electrodes prepared by the same protocol. Thus, the differences in charge-storage performances and kinetics in three different electrolytes are attributed, mainly, to the electrolyte ion characteristics. The ion migration in supercapacitors takes place at low-frequency region (below 100 Hz), and the diffusion occurs in the mid-frequency region [43]. Here, we estimated the ionic diffusion coefficient from the plot of Z' vs $\omega^{-0.5}$ (Fig. 4d). The slope of the curve is called the Warburg coefficient (σ) [55]. The estimated σ-values of electrode in 6 M KOH, 1 M H_2SO_4, and 1 M Na_2SO_4 are 198 Ω/s, 554 Ω/s, and 1720 Ω/s$^{0.5}$, respectively. This suggests better compatibility of 6 M KOH electrolyte with the [3]Ph-cumulene wrapped PMMA film in terms of ion diffusion.

The stability of the [3]Ph-cumulene-based supercapacitors in the aggressive electrolytes has been verified by comparing the Raman spectra of the electrodes before and after electrochemical measurements (Fig. 5a). For the Raman spectra of [3]Ph-cumulene wrapped PMMA film after the electrochemical investigation, the device was disassembled, the electrodes were washed in water several times to remove the electrolyte residue, and dried at open environment. The spectra are all similar, and the Raman peaks of the [3]Ph-cumulene remain effectively unchanged after immersion in the different electrolytes. These results confirm that the PMMA matrix is highly effective in the stabilization and protection of the [3]Ph-cumulene even in highly alkaline and basic environments. A more detailed investigation has been done considering the relative area of the ECC peak of [3]Ph-cumulene (2035 cm^{-1}, related to the *sp*-carbon skeleton) with respect to the area of the signal of the phenyl group (1593 cm^{-1}, related to the sp^2 endgroup) in thin films before and after the electrochemical measurements. Variations in this value would document the degradation of [3]Ph-cumulene during the charge-discharge experiment. Fig. 5b shows that the relative ratio of signal ECC/phenyl is found to be between 2.12 and 2.3 for the [3]Ph-cumulene before and after the electrochemical investigations, respectively. The relative reduction in the ECC signal is only 4.3 % and 7.2 % in the case of 1 M H_2SO_4 and 6 M KOH, respectively, and emphasizes the excellent structural stability of *sp*-carbon as electrodes. Moreover, we have carried out the morphological investigation of [3]Ph-PMMA film before and after electrochemistry, and the results reveal almost negligible changes in the morphology of the film after electrochemical performances (Figs. S2(a–b)).

4. Conclusion

We have investigated the electrochemical charge-storage properties and frequency response of PMMA-wrapped cumulenic *sp*-carbon atomic wires in supercapacitor devices using three different aqueous electrolytes, namely, 1 M Na_2SO_4, 1 M H_2SO_4, and 6 M KOH. The electrode material delivered higher areal capacitance with fast frequency

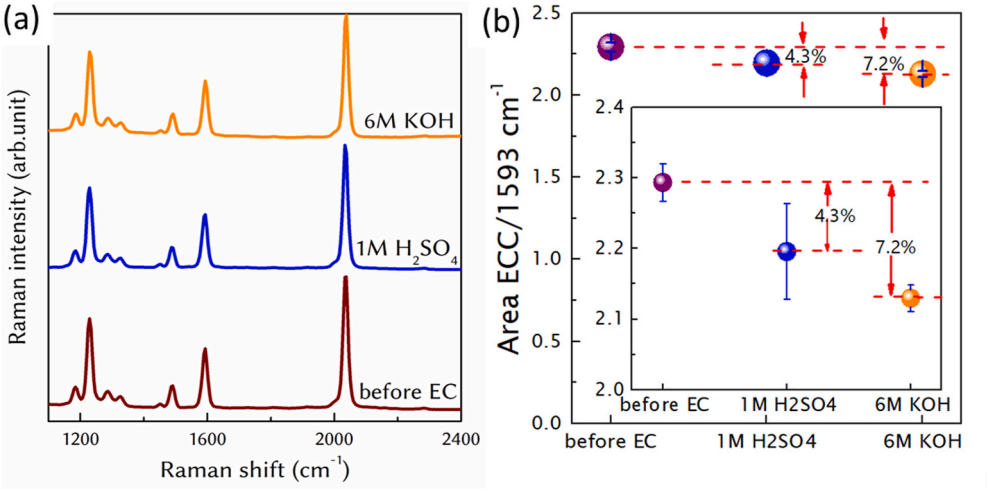

Fig. 5. (a) Raman spectra and (b) evolution of the ratio of Raman signals of ECC/phenyl (at 2035 and 1593 cm^{-1}, respectively) of [3]Ph-cumulene wrapped PMMA film before and after the electrochemical measurements in the different aqueous electrolytes. (A colour version of this figure can be viewed online.)

response, rate performance, cycle stability, higher negative phase angle, and smaller time constants in 6 M KOH compared to that in 1 M Na_2SO_4 and 1 M H_2SO_4. This performance is attributed to the better ionic diffusion, and balanced double-layer capacitance and pseudo-capacitance in 6 M KOH electrolyte. Analysis after electrochemical measurements confirmed that the active component [3]Ph-cumulene, does not appreciably degrade, even under the rigorous conditions of electrochemical charge/discharge. Thus [3]Ph-cumulenic *sp*-carbon atomic wires hold great promise as an electrode material for electrochemical energy storage and AC-line filtering applications, and they are anticipated as an electrolyte additives for the Li-ion and Na-ion battery applications [62,63].

CRediT authorship contribution statement

Subrata Ghosh: Writing – original draft, Supervision, Resources, Methodology, Investigation, Funding acquisition, Formal analysis, Data curation, Conceptualization. **Massimiliano Righi:** Investigation, Data curation. **Simone Melesi:** Writing – review & editing, Validation, Supervision, Methodology, Investigation, Formal analysis, Conceptualization. **Yu Qiu:** Methodology. **Rik R. Tykwinski:** Writing – review & editing, Methodology, Funding acquisition. **Carlo S. Casari:** Writing – review & editing, Supervision, Resources, Project administration, Funding acquisition, Conceptualization.

Notes

The authors declare no competing financial interest.

Data availability

All the data of this study are available in the main manuscript and the Supplementary Information.

Declaration of competing interest

The authors declare that they have no known competing financial interests or personal relationships that could have appeared to influence the work reported in this paper.

Acknowledgement

S.G thanks Horizon Europe (HORIZON) for the Marie Sklodowska-Curie Fellowship (grant no. 101067998-ENHANCER). C.S.C. acknowledges partial funding from the European Research Council (ERC) under the European Union's Horizon 2020 Research and Innovation Program ERC Consolidator Grant (ERC CoG2016 EspLORE Grant Agreement 724610, website: www.esplore.polimi.it). C.S.C. also acknowledges funding by the project funded under the National Recovery and Resilience Plan (NRRP), Mission 4 Component 2 Investment 1.3 Call for Tender 1561 of October 11, 2022 of Ministero dell'Università e della Ricerca (MUR), funded by the European Union NextGenerationEU Award Project Code Concession Decree 1561 of October 11, 2022 adopted by Ministero dell'Università e della Ricerca (MUR), CUP D43C22003090001, Project "Network 4 Energy Sustainable Transition (NEST)". R.R.T. acknowledges funding from the Natural Sciences and Engineering Research Council of Canada (RGPIN-2023-04000) and the Canada Foundation for Innovation (CFI). We also acknowledge, highly appreciate and grateful to anonymous reviewers for their time, and valuable and constructive suggestions.

Appendix A. Supplementary data

Supplementary data to this article can be found online at https://doi.org/10.1016/j.carbon.2024.119952.

References

[1] P. Simon, Y. Gogotsi, B. Dunn, Where do batteries end and supercapacitors begin? Science 343 (2014) 1210–1211, https://doi.org/10.1126/science.1249625.
[2] S. Ghosh, S. Barg, S.M. Jeong, K.K. Ostrikov, Heteroatom-doped and oxygen-functionalized nanocarbons for high-performance supercapacitors, Adv. Energy Mater. 10 (2020) 2001239, https://doi.org/10.1002/aenm.202001239.
[3] S. Ghosh, S.R. Polaki, A. Macrelli, C.S. Casari, S. Barg, S.M. Jeong, K. Ken Ostrikov, Nanoparticle-enhanced multifunctional nanocarbons—recent advances on electrochemical energy storage applications, J. Phys. D Appl. Phys. 55 (2022) 413001, https://doi.org/10.1088/1361-6463/ac7bb5.
[4] H. Peng, B. Yao, X. Wei, T. Liu, T. Kou, P. Xiao, Y. Zhang, Y. Li, Pore and heteroatom engineered carbon foams for supercapacitors, Adv. Energy Mater. 9 (2019) 1803665, https://doi.org/10.1002/aenm.201803665.
[5] M. Inagaki, H. Konno, O. Tanaike, Carbon materials for electrochemical capacitors, J. Power Sources 195 (2010) 7880–7903, https://doi.org/10.1016/j.jpowsour.2010.06.036.
[6] A. Philip, A. Ruban Kumar, Recent advancements and developments employing 2D-materials in enhancing the performance of electrochemical supercapacitors: a review, Renew. Sustain. Energy Rev. 182 (2023) 113423, https://doi.org/10.1016/j.rser.2023.113423.
[7] A.F. Burke, J. Zhao, Past, present and future of electrochemical capacitors: technologies, performance and applications, J. Energy Storage 35 (2021) 102310, https://doi.org/10.1016/j.est.2021.102310.
[8] Y. Zhu, S. Murali, M.D. Stoller, K.J. Ganesh, W. Cai, P.J. Ferreira, A. Pirkle, R. M. Wallace, K.A. Cychosz, M. Thommes, Carbon-based supercapacitors produced by activation of graphene, Science 332 (2011) 1537–1541.
[9] K. Honda, T.N. Rao, D.A. Tryk, A. Fujishima, M. Watanabe, K. Yasui, H. Masuda, Impedance characteristics of the nanoporous honeycomb diamond electrodes for electrical double-layer capacitor applications, J. Electrochem. Soc. 148 (2001) A668, https://doi.org/10.1149/1.1373450.
[10] M. Yoshimura, K. Honda, R. Uchikado, T. Kondo, T.N. Rao, D.A. Tryk, A. Fujishima, Y. Sakamoto, K. Yasui, H. Masuda, Electrochemical characterization of nanoporous honeycomb diamond electrodes in non-aqueous electrolytes, Diam. Relat. Mater. 10 (2001) 620–626, https://doi.org/10.1016/S0925-9635(00)00381-2.
[11] S. Karmakar, S. Taqy, R. Droopad, R.K. Trivedi, B. Chakraborty, A. Haque, Highly stable electrochemical supercapacitor performance of self-assembled ferromagnetic Q-carbon, ACS Appl. Mater. Interfaces 15 (2023) 8305–8318, https://doi.org/10.1021/acsami.2c20202.
[12] P.B. Sorokin, H. Lee, L.Y. Antipina, A.K. Singh, B.I. Yakobson, Calcium-decorated carbyne networks as hydrogen storage media, Nano Lett. 11 (2011) 2660–2665, https://doi.org/10.1021/nl200721v.
[13] M. Liu, V.I. Artyukhov, H. Lee, F. Xu, B.I. Yakobson, Carbyne from first principles: chain of C atoms, a nanorod or a nanorope, ACS Nano 7 (2013) 10075–10082, https://doi.org/10.1021/nn404177r.
[14] F. Yang, Z. Zheng, Y. He, P. Liu, G. Yang, A new wide bandgap semiconductor: carbyne nanocrystals, Adv. Funct. Mater. 31 (2021), https://doi.org/10.1002/adfm.202104254.
[15] V.I. Artyukhov, M. Liu, B.I. Yakobson, Mechanically induced metal–insulator transition in carbyne, Nano Lett. 14 (2014) 4224–4229, https://doi.org/10.1021/nl5017317.
[16] C.S. Casari, M. Tommasini, R.R. Tykwinski, A. Milani, Carbon-atom wires: 1-D systems with tunable properties, Nanoscale 8 (2016) 4414–4435, https://doi.org/10.1039/C5NR06175J.
[17] Y. Gao, R.R. Tykwinski, Advances in polyynes to model carbyne, Acc. Chem. Res. 55 (2022) 3616–3630, https://doi.org/10.1021/acs.accounts.2c00662.
[18] S. Peggiani, P. Marabotti, R.A. Lotti, A. Facibeni, P. Serafini, A. Milani, V. Russo, A. Li Bassi, C.S. Casari, Solvent-dependent termination, size and stability in polyynes synthesized via laser ablation in liquids, Phys. Chem. Chem. Phys. 22 (2020) 26312–26321, https://doi.org/10.1039/D0CP04132G.
[19] B. Pigulski, N. Gulia, P. Męcik, R. Wieczorek, A. Arendt, S. Szafert, Crystal engineering of 1-halopolyynes by end-group manipulation, Cryst. Growth Des. 19 (2019) 6542–6551, https://doi.org/10.1021/acs.cgd.9b00987.
[20] F. Cataldo, O. Ursini, A. Milani, C.S. Casari, One-pot synthesis and characterization of polyynes end-capped by biphenyl groups (α,ω-biphenylpolyynes), Carbon N. Y. 126 (2018) 232–240, https://doi.org/10.1016/j.carbon.2017.09.098.
[21] S. Melesi, P. Marabotti, A. Milani, B. Pigulski, N. Gulia, P. Pińkowski, S. Szafert, M. Del Zoppo, C. Castiglioni, C.S. Casari, Impact of halogen termination and chain length on π-electron conjugation and vibrational properties of halogen-terminated polyynes, J. Phys. Chem. A 128 (2024) 2703–2716, https://doi.org/10.1021/acs.jpca.3c07915.
[22] A. Milani, M. Tommasini, V. Russo, A. Li Bassi, A. Lucotti, F. Cataldo, C.S. Casari, Raman spectroscopy as a tool to investigate the structure and electronic properties of carbon-atom wires, Beilstein J. Nanotechnol. 6 (2015) 480–491, https://doi.org/10.3762/bjnano.6.49.
[23] S. Peggiani, A. Facibeni, A. Milani, C. Castiglioni, V. Russo, A. Li Bassi, C.S. Casari, In situ synthesis of polyynes in a polymer matrix via pulsed laser ablation in a liquid, Mater. Adv. 1 (2020) 2729–2736, https://doi.org/10.1039/D0MA00545B.
[24] S. Okada, M. Fujii, S. Hayashi, Immobilization of polyynes adsorbed on Ag nanoparticle aggregates into poly(vinyl alcohol) films, Carbon N. Y. 49 (2011) 4704–4709, https://doi.org/10.1016/j.carbon.2011.06.074.
[25] K. An, G. Wei, G. Qi, L. Sheng, L. Yu, W. Ren, X. Zhao, Stability improvement of C8H2 and C10H2 embedded in poly(vinyl alcohol) films with adsorption on gold nanoparticles, Chem. Phys. Lett. 637 (2015) 71–76, https://doi.org/10.1016/j.cplett.2015.07.051.

[26] F. Cataldo, Stability of polyynes in air and their degradation by ozonolysis, Polym. Degrad. Stabil. 91 (2006) 317–323, https://doi.org/10.1016/j.polymdegradstab.2005.04.046.
[27] D. Heymann, Thermolysis of the polyyne C8H2 in hexane and methanol: Experimental and theoretical study, Carbon N. Y. 43 (2005) 2235–2242, https://doi.org/10.1016/j.carbon.2005.03.038.
[28] C.S. Casari, A. Li Bassi, L. Ravagnan, F. Siviero, C. Lenardi, P. Piseri, G. Bongiorno, C.E. Bottani, P. Milani, Chemical and thermal stability of carbyne-like structures in cluster-assembled carbon films, Phys. Rev. B 69 (2004) 075422, https://doi.org/10.1103/PhysRevB.69.075422.
[29] L.G. Bettini, F. Della Foglia, P. Piseri, P. Milani, Interfacial properties of a carbyne-rich nanostructured carbon thin film in ionic liquid, Nanotechnology 27 (2016) 115403, https://doi.org/10.1088/0957-4484/27/11/115403.
[30] A.D. Scaccabarozzi, A. Milani, S. Peggiani, S. Pecorario, B. Sun, R.R. Tykwinski, M. Caironi, C.S. Casari, A field-effect transistor based on cumulenic sp-carbon atomic wires, J. Phys. Chem. Lett. 11 (2020) 1970–1974, https://doi.org/10.1021/acs.jpclett.0c00141.
[31] S. Pecorario, A.D. Scaccabarozzi, D. Fazzi, E. Gutiérrez-Fernández, V. Vurro, L. Maserati, M. Jiang, T. Losi, B. Sun, R.R. Tykwinski, C.S. Casari, M. Caironi, Stable and solution-processable cumulenic sp-carbon wires: a new paradigm for organic electronics, Adv. Mater. 34 (2022), https://doi.org/10.1002/adma.202110468.
[32] A.P. Piedade, L. Cangueiro, Influence of carbyne content on the mechanical performance of nanothick amorphous carbon coatings, Nanomaterials 10 (2020), https://doi.org/10.3390/nano10040780.
[33] V.K. Mariappan, K. Krishnamoorthy, P. Pazhamalai, S. Sahoo, S.-J. Kim, Carbyne-enriched carbon anchored on nickel foam: a novel binder-free electrode for supercapacitor application, J. Colloid Interface Sci. 556 (2019) 411–419, https://doi.org/10.1016/j.jcis.2019.08.055.
[34] P. Marabotti, M. Tommasini, C. Castiglioni, P. Serafini, S. Peggiani, M. Tortora, B. Rossi, A. Li Bassi, V. Russo, C.S. Casari, Electron-phonon coupling and vibrational properties of size-selected linear carbon chains by resonance Raman scattering, Nat. Commun. 13 (2022) 5052, https://doi.org/10.1038/s41467-022-32801-3.
[35] S. Ghosh, M. Righi, A. Macrelli, G. Divitini, D. Orecchia, A. Maffini, F. Goto, G. Bussetti, D. Dellasega, V. Russo, A. Li Bassi, C.S. Casari, Ballistic-aggregated carbon nanofoam in target-side of pulsed laser deposition for energy storage applications, ChemSusChem (2024) 202400755, https://doi.org/10.1002/cssc.202400755.
[36] C.D. Tschannen, G. Gordeev, S. Reich, L. Shi, T. Pichler, M. Frimmer, L. Novotny, S. Heeg, Raman scattering cross section of confined carbyne, Nano Lett. 20 (2020) 6750–6755, https://doi.org/10.1021/acs.nanolett.0c02632.
[37] D. Wendinger, R.R. Tykwinski, Odd [n]cumulenes (n = 3, 5, 7, 9): synthesis, characterization, and reactivity, Acc. Chem. Res. 50 (2017) 1468–1479, https://doi.org/10.1021/acs.accounts.7b00164.
[38] S. Ghosh, T. Mathews, B. Gupta, A. Das, N. Gopala Krishna, M. Kamruddin, Supercapacitive vertical graphene nanosheets in aqueous electrolytes, Nano-Structures & Nano-Objects 10 (2017) 42–50, https://doi.org/10.1016/j.nanoso.2017.03.008.
[39] S. Ghosh, G. Pagani, M. Righi, C. Hou, V. Russo, C.S. Casari, One-step pulsed laser deposition of carbon/metal oxynitride composites for supercapacitor application, J. Phys. D Appl . Phys. 57 (2024) 495305, https://doi.org/10.1088/1361-6463/ad76bc.
[40] Z. Wang, Z. Li, Z. Zou, Application of binder-free TiOxN1−x nanogrid film as a high-power supercapacitor electrode, J. Power Sources 296 (2015) 53–63, https://doi.org/10.1016/j.jpowsour.2015.07.040.
[41] Z.-H. Huang, T.-Y. Liu, Y. Song, Y. Li, X.-X. Liu, Balancing the electrical double layer capacitance and pseudocapacitance of hetero-atom doped carbon, Nanoscale 9 (2017) 13119–13127, https://doi.org/10.1039/C7NR04234E.
[42] S. Ardizzone, G. Fregonara, S. Trasatti, "Inner" and "outer" active surface of RuO2 electrodes, Electrochim. Acta 35 (1990) 263–267, https://doi.org/10.1016/0013-4686(90)85068-X.
[43] S. Zhang, B. Li, C. Cui, W. Qian, Y. Jin, The progress and comprehensive analysis of supercapacitors for alternating current line filtering: a review, Batter. Supercaps. 6 (2023), https://doi.org/10.1002/batt.202200566.
[44] M. Cai, R.A. Outlaw, R.A. Quinlan, D. Premathilake, S.M. Butler, J.R. Miller, Fast response, vertically oriented graphene nanosheet electric double layer capacitors synthesized from C2H2, ACS Nano 8 (2014) 5873–5882.
[45] T. Lin, I.-W. Chen, F. Liu, C. Yang, H. Bi, F. Xu, F. Huang, Nitrogen-doped mesoporous carbon of extraordinary capacitance for electrochemical energy storage, Science 350 (2015) 1508–1513, https://doi.org/10.1126/science.aab3798.
[46] P.L. Taberna, P. Simon, J.F. Fauvarque, Electrochemical characteristics and impedance spectroscopy studies of carbon-carbon supercapacitors, J. Electrochem. Soc. 150 (2003) A292, https://doi.org/10.1149/1.1543948.
[47] N. Islam, M.N.F. Hoque, W. Li, S. Wang, J. Warzywoda, Z. Fan, Vertically edge-oriented graphene on plasma pyrolyzed cellulose fibers and demonstration of kilohertz high-frequency filtering electrical double layer capacitors, Carbon N. Y. 141 (2019) 523–530, https://doi.org/10.1016/J.CARBON.2018.10.012.
[48] T. Nathan-Walleser, I. Lazar, M. Fabritius, F.J. Tölle, Q. Xia, B. Bruchmann, S. S. Venkataraman, M.G. Schwab, R. Mülhaupt, 3D micro-extrusion of graphene-based active electrodes: towards high-rate AC line filtering performance electrochemical capacitors, Adv. Funct. Mater. 24 (2014) 4706–4716, https://doi.org/10.1002/adfm.201304151.
[49] J. Xue, Z. Gao, L. Xiao, T. Zuo, J. Gao, D. Li, L. Qu, An ultrafast supercapacitor based on 3D ordered porous graphene film with AC line filtering performance, ACS Appl. Energy Mater. 3 (2020) 5182–5189, https://doi.org/10.1021/acsaem.9b02458.
[50] Z. Bo, C. Xu, H. Yang, H. Shi, J. Yan, K. Cen, K. Ostrikov, Hierarchical, vertically-oriented carbon nanowall foam supercapacitor using room temperature ionic liquid mixture for AC line filtering with ultrahigh energy density, Chemelectrochem 6 (2019) 2167–2173, https://doi.org/10.1002/celc.201801825.
[51] H. Tang, K. Xia, J. Lu, J. Fu, Z. Zhu, Y. Tian, Y. Wang, M. Liu, J. Chen, Z. Xu, Y. Guo, R. Khatoon, H. Chen, Z. Ye, NiTe2-based electrochemical capacitors with high-capacitance AC line filtering for regulating TENGs to steadily drive LEDs, Nano Energy 84 (2021) 105931, https://doi.org/10.1016/j.nanoen.2021.105931.
[52] Y.J. Kang, Y. Yoo, W. Kim, 3-V solid-state flexible supercapacitors with ionic-liquid-based polymer gel electrolyte for AC line filtering, ACS Appl. Mater. Interfaces 8 (2016) 13909–13917, https://doi.org/10.1021/acsami.6b02690.
[53] M. Kim, B.-K. Ju, J.G. Kang, Hierarchical multiscale engineered Fe 3 O 4/Ni electrodes with ultrafast supercapacitive energy storage for alternate current line-filtering, Small Sci 3 (2023), https://doi.org/10.1002/smsc.202200074.
[54] D. Zhao, K. Jiang, J. Li, X. Zhu, C. Ke, S. Han, E. Kymakis, X. Zhuang, Supercapacitors with alternating current line-filtering performance, BMC Mater 2 (2020) 1–20, https://doi.org/10.1186/s42833-020-0009-z.
[55] Y. Yuan, C. Zhan, K. He, H. Chen, W. Yao, S. Sharifi-Asl, B. Song, Z. Yang, A. Nie, X. Luo, H. Wang, S.M. Wood, K. Amine, M.S. Islam, J. Lu, R. Shahbazian-Yassar, The influence of large cations on the electrochemical properties of tunnel-structured metal oxides, Nat. Commun. 7 (2016) 13374, https://doi.org/10.1038/ncomms13374.
[56] M. Zhao, J. Nie, H. Li, M. Xia, M. Liu, Z. Zhang, X. Liang, R. Qi, Z.L. Wang, X. Lu, High-frequency supercapacitors based on carbonized melamine foam as energy storage devices for triboelectric nanogenerators, Nano Energy 55 (2019) 447–453, https://doi.org/10.1016/j.nanoen.2018.11.016.
[57] S. Yu, K.J. Sankaran, S. Korneychuk, J. Verbeeck, K. Haenen, X. Jiang, N. Yang, High-performance supercabatteries using graphite@diamond nano-needle capacitor electrodes and redox electrolytes, Nanoscale 11 (2019) 17939–17946, https://doi.org/10.1039/C9NR07037K.
[58] J.R. Miller, R.A. Outlaw, B.C. Holloway, Graphene double-layer capacitor with ac line-filtering performance, Science 329 (2010) 1637–1639, https://doi.org/10.1126/science.1194372.
[59] Y.J. Kang, Y. Yoo, W. Kim, 3-V solid-state flexible supercapacitors with ionic-liquid-based polymer gel electrolyte for AC line filtering, ACS Appl. Mater. Interfaces 8 (2016) 13909–13917, https://doi.org/10.1021/acsami.6b02690.
[60] Z.J. Han, C. Huang, S.S. Meysami, D. Piche, D.H. Seo, S. Pineda, A.T. Murdock, P. S. Bruce, P.S. Grant, N. Grobert, High-frequency supercapacitors based on doped carbon nanostructures, Carbon N. Y. 126 (2018) 305–312, https://doi.org/10.1016/j.carbon.2017.10.014.
[61] Z. Zhang, Z. Wang, F. Wang, T. Qin, H. Zhu, P. Liu, G. Zhao, X. Wang, F. Kang, L. Wang, C. Yang, A laser-processed carbon-titanium carbide heterostructure electrode for high-frequency micro-supercapacitors, Small 19 (2023) 2300747, https://doi.org/10.1002/smll.202300747.
[62] Y. Huang, B. Shao, F. Han, Li alloy anodes for high-rate and high-areal-capacity solid-state batteries, J. Mater. Chem. A 10 (2022) 12350–12358, https://doi.org/10.1039/D2TA02339C.
[63] J. Yue, Y. Huang, S. Liu, J. Chen, F. Han, C. Wang, Rational designed mixed-conductive sulfur cathodes for all-solid-state lithium batteries, ACS Appl. Mater. Interfaces 12 (2020) 36066–36071, https://doi.org/10.1021/acsami.0c08564.